Chemical Engineering Journal 402 (2020) 125640

Contents lists available at ScienceDirect

Chemical Engineering Journal

journal homepage: www.elsevier.com/locate/cej

Estimating surface electric fields using reactive formic acid probes and SEM image brightness analysis

Jake T. Gray[a], Kriti Agarwal[b], Jeong-Hyun Cho[b], Jung-Il Yang[c], Su Ha[a,*]

[a] The Gene and Linda Voiland School of Chemical Engineering and Bioengineering, Washington State University, WA 99164, USA
[b] Department of Electrical and Computer Engineering, University of Minnesota, Minneapolis, MN 55455, USA
[c] Clean Fuel Laboratory, Korea Institute of Energy Research, Daejeon 305-343, Republic of Korea

HIGHLIGHTS

- Electric field enhanced catalytic decomposition of gas-phase formic acid.
- Reaction used to estimate applied field strength at catalyst active site.
- COMSOL model used to predict field structure across Ni foam catalyst.
- Applied field is visualized by electron microscopy differential image brightness.

GRAPHICAL ABSTRACT

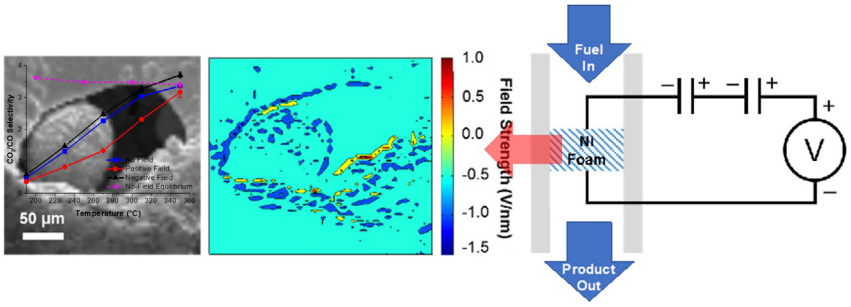

ARTICLE INFO

Keywords:
Formic acid decomposition
Surface electric field
Selectivity enhancement
SEM brightness imaging
COMSOL model

ABSTRACT

By changing the electrical bias imposed on a Ni catalyst attached to an external circuit, the selectivity of catalytic formic acid decomposition is shown to change—favoring CO_2/H_2 production under negative bias and CO/H_2O production under positive bias. A method for estimating the strength of externally generated surface electric fields by measuring this selectivity change is presented and used to approximate field strengths on the order of 0.20 V/nm. A COMSOL model of the catalyst was created which indicated that the presence of Ni particles increased field strength and uniformity across the catalyst. Comparing this model to SEM imaging of the catalyst verified that the field strengths are highest on the surface of the catalyst particles, pore edges, and microscopic defects. The methods developed herein may be useful to future reaction engineers seeking to incorporate applied electric fields into process designs.

1. Introduction

The thermodynamic effects of an electric field on chemical reactions were outlined by Bergmann et al. in a 1963 paper which related the strength of the field (F) to the equilibrium constant (K):

$$\frac{\partial(\ln(K))}{\partial F} = \frac{\Delta m}{RT} \quad (1)$$

where R is the universal gas constant, T is the reaction temperature, and Δm is the change in the electric moment of the molecules over the course of the reaction. The value of Δm is expressed as:

$$\Delta m = \Delta\mu + F\Delta\alpha + \cdots \quad (2)$$

where μ is the dipole moment, α is the polarizability of the molecules, and the hyperpolarizability terms have been truncated [1]. Eq. (1) has been extensively cited by researchers, but it is rarely applied directly to the analysis of reactive chemical systems in an electric field due to the difficulty of accounting for all possible reaction pathways available for

* Corresponding author.

https://doi.org/10.1016/j.cej.2020.125640
Received 7 February 2020; Received in revised form 22 May 2020; Accepted 23 May 2020
Available online 28 May 2020

the given catalytic system [2–7]. Strong electric fields can also influence reaction kinetics [8–10]. Reaction rate constants as a function of field strength can be expressed using the Arrhenius equation:

$$k(F) = A(F)e^{-\frac{E_a(F)}{RT}} \quad (3)$$

where k is the rate constant, A is the frequency factor, and E_a is the activation energy. The frequency factor is changed by electric fields due to (anti)alignment of the dipole moments of molecules in the field and changes in the activation energy are due to (de)stabilization of reactants, transition states, and products in the field from distortion of their molecular orbitals.

Prior experimental attempts at performing chemistry under the influence of strong electric fields have been largely limited to high-vacuum, low-throughput systems where dielectric breakdown (i.e. plasma generation) is avoided. The field ion microscope is a classic example of such tests, where electric fields on the order of 10–100 V/nm can be generated on a fine metal tip which serves as the catalyst surface [11–16]. These tests are always conducted under high vacuum over a single "grain" of catalyst configured as a metal probe. Thus, although these experiments are scientifically instructive, they are inherently limited in their scalability and applicability. Scanning tunneling microscopes have also been used to similar effect, with similar drawbacks [17–20].

Attempts at upscaling this process have been ongoing for decades, but progress has been slow. Several issues still exist which prevent the use of applied electric fields as general reaction engineering tools including gaps in our basic understanding of chemistry in strong fields, a dearth of suitable reactor designs, and a lack of tools needed for characterizing and designing reactors. Especially, progress on the reactor design front is slow due to a general lack of design principles stemming from a disconnect between chemical reaction engineering principles and electrical physics.

The most commonly used applied electric field reactor in the literature since 2000 has been the "probe-bed-probe" reactor (PBPR) shown in Fig. 1. This design has shown remarkable success in improving yields and conversions for a wide range of reactions over many different catalysts [21]. Despite these apparent successes, however, the reactor has yet to be properly characterized which can make a connection to the few models available very difficult. Questions still exist as to what the strength and structure of the field is at the catalyst surface. This is not a trivial question to answer but, without at least an approximation, we cannot be sure of the accuracy of our assumptions about the process. For example, the PBPR is assumed to impress some electric field upon the catalyst bed. However, every instance of successful PBPR use requires that current flows between the probes [21]. Since there is often a gap of several millimeters between the probes and the catalyst bed, the question arises as to how this current develops. Without a thorough characterization and connection to fundamental models, we cannot be sure that this phenomenon is not due to thermal activation from Joule heating of the catalyst, plasma generation, or electric-field-adjacent phenomenon like the non-Faradaic electrochemical modification of catalytic activity (NEMCA) first observed by Stoukides and Vayenas in 1981 [22,23].

This points to another direct obstacle preventing the successful incorporation of strong electric fields in heterogeneous catalytic processes: the risk of generating plasma. Although plasma is not inherently a bad thing—plasma reactors similar in design to the PBPR are often used in waste remediation [24]—it nevertheless can be detrimental to studies of applied electric fields. In terms of scientific value, it is difficult to uncouple the effects of the electric field established in the reactor from those effects that arise due to high-energy impacts from radicals or other plasma species presented in the bulk gas phase. Additionally, from an engineering perspective, the selectivity of plasma reactions is difficult to control as it is a high-energy process which activates molecules indiscriminately [25].

We have attempted in our past work to carefully uncouple the various effects associated with applying an electric field under atmospheric conditions. These trials exploited the intrinsic physics of circuits, namely the weak charge distributions that arise at the surface of wires integrated into a circuit [26–30]. Discharge was not observed for the same reason that it is not generated in any other normal circuit—in the absence of a counterelectrode or nearby ground, there is no path for electrons to flow. Joule heating and Faraday reactions were controlled by ensuring no current flowed through the electrified circuit. This was done by incorporating other external circuit elements such as strong resistors or capacitors. The reactor used in the present study, shown in Fig. 2, was used in several other studies on the chemistry of methane steam reforming over nickel and compared to detailed DFT and microkinetic models to good agreements [8–10,31]. Although we

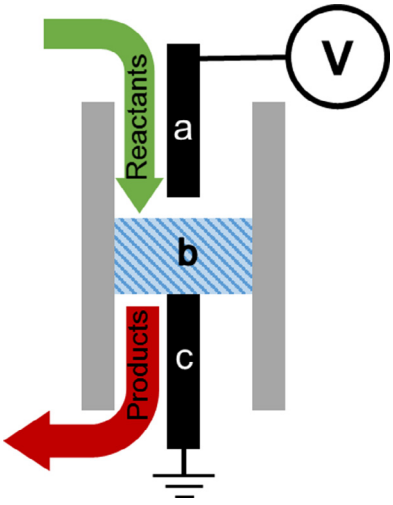

Fig. 1. Schematic representation of a commonly used PBPR reactor. Stainless steel probes (a) and (c) are fixed above and below a catalyst bed (b) consisting of loose catalyst grains, typically metal particles on nonconductive supports like silica or alumina, such that the stainless steel probe (c) is (typically) in contact with the bottom portion of the catalyst bed and the stainless steel probe (a) is set some fixed distance from the upper surface of the catalyst bed (usually 0–5 mm). Variable voltages are applied to the stainless steel probe (a) such that a constant current (usually 3–5 mA) flows between two metal probes (a) and (b).

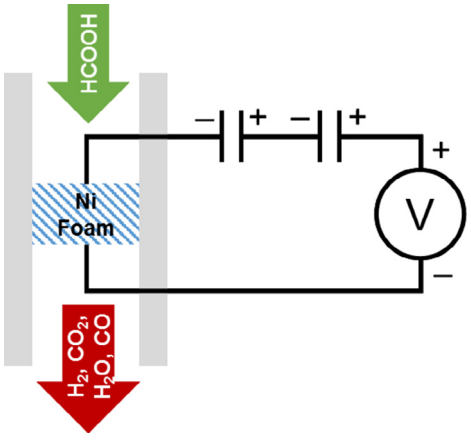

Fig. 2. Schematic representation of the reactor configuration and external circuit used for the surface electric field assisted formic acid reforming tests. Two capacitors connected in series (to avoid potential overvoltage issues; manufacturer spec to 200 V ± 10 V) and a DC power source comprised the external circuit. Surface charges on the wire connecting the capacitor terminal to the power source generates the applied surface electric field over the Ni foam reactor—in this case, a negative surface field.

observed many points of encouraging agreement between theory and experiment, there were some observations that could not be explained which suggest either our model is incomplete, our application of the model is incorrect, our understanding of the reactor is insufficient, or some combination of these factors.

In the present work, we use the simpler chemistry of formic acid decomposition to directly estimate the surface electric fields generated over a nickel catalyst inserted into an electric circuit consisting of a DC power source and a capacitor. Formic acid (HCOOH) decomposes via two pathways into CO and H_2O (dehydration) or CO_2 and H_2 (decarboxylation):

Decarboxylation $HCOOH \rightarrow H_2 + CO_2$ (Reaction 1)

Decarboxylation $HCOOH \rightarrow H_2\ O + CO$ (Reaction 2)

The formic acid decomposition reaction was chosen for its low number of possible reaction pathways as a unimolecular decomposition. It was also considered a good candidate for the intrinsic dipole moment of the reactant, which should interact strongly with the field as predicted by Eq. (1). The approach taken in this work is to estimate the behavior of this reaction in a manner that requires less resources and time than developing a full DFT or microkinetic model and is, hopefully, more accessible to future reaction engineers or reactor designers. To that end, this paper focuses on the use of Eq. (1) in a thermodynamic approach. In addition to demonstrating the predictive power of Eq. (1) for catalytic reactions (albeit in limited situations), we also propose a method by which these equations can be applied to estimate the magnitude of surface electric fields generated in the reactor from HCOOH decomposition experimental data. These predictions were compared to simple COMSOL models of our reactor. Finally, in order to validate the surface electric field structure predicted by the COMSOL model, we develop a method for visualizing the electric fields generated in our reactor using a scanning electron microscope. A brief description of the physical rationale behind the SEM brightness imaging technique is provided in the Supplementary Information (SI, Figs. S1 and S2).

2. Methods

2.1. Reactor fabrication

Reactors were constructed using Ni foam catalysts (Goodfellow, 99.5% purity, 95% porosity) cut into 7 mm disks to fit the inside of a quartz tube reactor. Ni microparticles (Alfa Aesar, 99.98%, ~95 μm diameter) were sintered to each disk by smearing a mixture of 2:1 (by weight) of particles and a viscous petroleum jelly (Heraeus) and heating to 850 °C in flowing H_2 and Ar for 4 h. Two lengths of Ag wire (Alfa Aesar, 99.9%, 0.01 mm gauge) were threaded through four holes punched into the edges of the disk (two holes each on diametrically opposing sides) and then through slits cut into the quartz tube 2.5 cm from either end. Ceramic paste (Aremco Ceramabond 538) was used to seal the holes. A single catalyst disk was used for all tests for later comparison with COMSOL model and SEM imaging. We simplified the design down to a single catalyst disk and incorporated the capacitor as shown in Fig. 2 in order to minimize possible sources of error. The more catalyst material used, the more difficult it is to construct two reactors in precisely the same manner. Even with a single disk, this is very difficult since the foam has natural variations, as do the particles, where they are placed (precisely), and so on. Still, this very simple construction allows for a relatively straightforward to produce a reactor that can be tested with greater confidence.

2.2. Selectivity tests

Reactors were fitted with ultratorr fittings (Swagelok) and connected to a gas delivery system consisting of a mass flow controller connected to a 4-way valve. Samples were pretreated in flowing H_2 and Ar (50%) at 800 °C for 30 min. Formic acid was delivered to the system by bubbling Ar at 60 sccm through a vial of liquid formic acid (Sigma Aldrich, 99%) maintained at 0 °C in an ice bath. The reactors were held at temperature by an external ceramic furnace controlled by PID temperature controller.

The surface electric fields were generated by connecting the Ag wire leads attached to the catalyst disk to one terminal of a capacitor and to the terminal of a DC power source (VOLTEQ) set to 200 V as shown in Fig. 2. The capacitor was included to limit the current flow and mitigate unwanted Faraday reactions. Field direction is controlled by connecting the leads to different capacitor/source terminals (e.g. negative terminals for negative fields).

2.3. COMSOL model

Simulations were carried out using COMSOL Multiphysics AC/DC module version 5.2a. The Ni foam was modelled as a square plate of length 10 mm and thickness 0.5 mm. To simplify the model, the pores were designed as 0.5 mm diameter circular holes spread uniformly across the plate with 0.5 mm between the holes. A silver (Ag) wire of diameter 0.2 mm was connected to the center of the Ni plate and held at an input voltage of 200 V. Cubic Ni microparticles with a length of 95 μm were placed at the center of each pore.

2.4. SEM brightness imaging

A single wired catalyst disk was attached to a standard SEM stub using an insulating polymer glue (Itoya O'Glue). The glue prevented the sample from contacting the grounded SEM stage. The catalyst was connected to an electrical feedthrough port attached to the SEM (FEI Quanta) which was, in turn, attached to the same capacitor and DC source used in the reactive probe experiments. A detail experimental setup (Fig. S3) and additional image processing details (Figs. S4–S6) are provided in the SI. Images were taken by fixing the brightness, contrast, accelerating voltage, beam intensity, and all other user-controlled parameters while changing the applied voltage from the DC source.

3. Results and discussion

3.1. Thermodynamics calculations

The Δμ and Δα values for the two formic acid decomposition reaction pathways are provided in Table 1.

Using the data in Table 1 and Eqs. (1) and (2), the changes in Gibbs energy expected can be directly computed for both reaction pathways when formic acid is subjected to a strong electric field. The results of these calculations over a range of temperatures are shown in Fig. 3. These show that a negative electric field will enhance the decarboxylation reaction (Reaction (1)) while the positive electric field will

Table 1
Calculating dipole moment and polarizability changes for the two possible reactions for HCOOH decomposition from tabulated data. Physical data taken from the CRC Handbook of Chemistry and Physics, 99th Edition.

Reaction	Dipole moment change (D)	Polarizability change ($Å^3$)
(1) $HCOOH \longrightarrow H_2 + CO_2$	(0.00 + 0.00) − (1.40) = −1.40	(0.8 + 2.9) − (3.4) = 0.3
(2) $HCOOH \longrightarrow H_2O + CO$	(1.80 + 0.14) − (1.40) = 0.54	(1.5 + 0.12) − (3.4) = −1.78

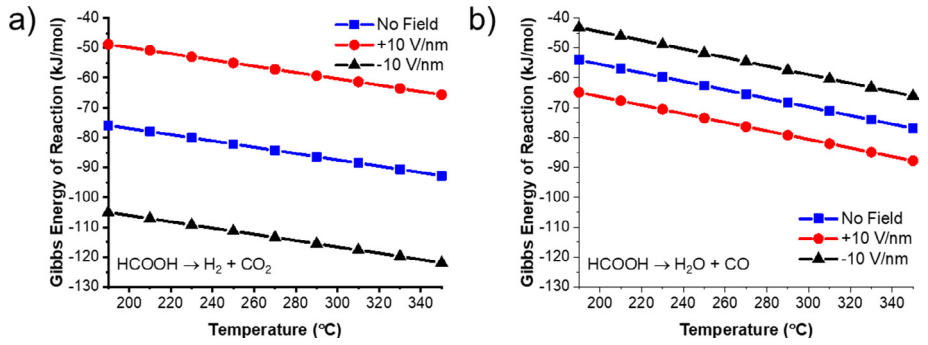

Fig. 3. Gibbs energy changes for (a) decarboxylation and (b) dehydration in the presence of electric fields of different directions.

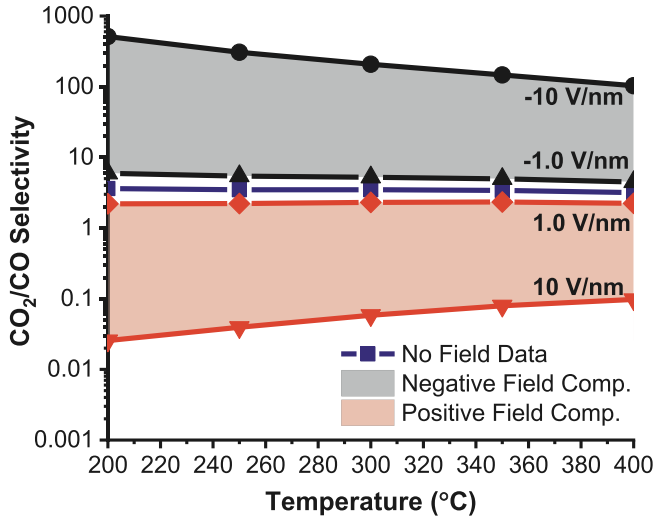

Fig. 4. Predicted changes in CO_2/CO selectivity upon application of various field directions and strengths. All the selectivity values are estimated using Eq. (9) except the data indicated by the blue squares. The blue line corresponds to the actual experimental selectivity data measured under no applied electric field. (For interpretation of the references to color in this figure legend, the reader is referred to the web version of this article.)

enhance the dehydration reaction (Reaction (2)).

Although these results are encouraging and provide support for the claim that the electric field should influence the reaction products, we wanted to develop a method by which this analysis could be directly applied to a simple reaction experiment. The selectivity, or the ratio of formic acid molecules undergoing decarboxylation to the number undergoing dehydration, was chosen for this analysis as it can be directly linked to the thermodynamics of a system.

3.2. Selectivity derivation

Let S be the ratio of the reaction rates of the two reactions indicated in Table 1 (r_1 and r_2):

$$S = \frac{r_1}{r_2} \tag{4}$$

Experimentally, these rates can be measured by determining the evolution rate of CO_2 and CO, respectively (see Section 2.2). Thus, the selectivity can be rewritten in terms of their concentrations in the effluent stream:

$$S = \frac{\dot{n}_{CO_2}}{\dot{n}_{CO}} = \frac{[CO_2]\dot{V}}{[CO]\dot{V}} = \frac{[CO_2]}{[CO]} \tag{5}$$

where $\dot{n}_x$ is the molar flow rate of species x and $\dot{V}$ is the volumetric flow rate exiting the reactor. The equilibrium constants for both reactions can be written in terms of concentration, as well, assuming standard conditions:

$$K_1 = \frac{[H_2][CO_2]}{[HCOOH]} = \frac{[CO_2]^2}{[HCOOH]} \tag{6}$$

$$K_2 = \frac{[H_2O][CO]}{[HCOOH]} = \frac{[CO]^2}{[HCOOH]} \tag{7}$$

Eqs. (6) and (7) were simplified assuming approximately equal concentrations of H_2 to CO_2 and H_2O to CO are produced during the reaction. Eqs. (5) through (7) can be combined to obtain the HCOOH decomposition selectivity in terms of the equilibrium constants of both reactions:

$$S = \sqrt{\frac{K_1}{K_2}} \tag{8}$$

Eq. (8) can then be combined with Eqs. (1) and (2) after integration with the boundary condition that $S'(F = 0) = S$:

$$S' = Se^{\frac{1}{2k_BT}\left((\Delta\mu_1 - \Delta\mu_2)F + \frac{1}{2}(\Delta\alpha_1 - \Delta\alpha_2)F^2\right)} \tag{9}$$

where S′ is the selectivity in the presence of an applied electric field.

3.3. Reactive formic acid probe estimates of surface field strength

Experimental selectivity tests over the Ni foam catalyst began with baseline no-field tests over the excess catalyst, as indicated by the blue line in Fig. 4. To ensure that thermodynamic equilibrium was reached, excess catalyst (several Ni foam disks) were loaded into the reactor, and reactions were conducted at various steady-state temperatures with 60 sccm Ar bubbled through 0 °C formic acid. Eq. (9) was then used to predict the influence of an applied electric field of various strengths and directions on the reaction selectivity. The results of these calculations are also shown in Fig. 4. These results indicate that positive fields should favor the production of CO/H_2O while negative fields should improve the production rates of CO_2/H_2. Although this is not new information (this was already obtained by direct analysis of Eq. (1) in Fig. 3), this analysis further provides information about the *magnitude* of the reaction selectivity change as a function of both the field strength and reaction temperature. Thus, by simply measuring the change in experimental selectivity as fields are applied, the surface electric field strengths generated near the catalyst active sites can be approximated using Fig. 4 (or directly solving Eq. (9) for the applied electric field (F) with the experimentally measured selectivity (S′) value).

Fig. 5 shows the experimental selectivity data from the electric field enhanced reactor with one Ni foam disk as a function of its operating temperature under the various applied electric fields (i.e., positive field, no field, and negative field). It also shows the experimental equilibrium selectivity data with the zero applied electric field (purple stars). These data were collected over excess catalyst and represent the maximum selectivity values possible across the low surface area Ni foam catalyst. Although these values are used as target values for determining

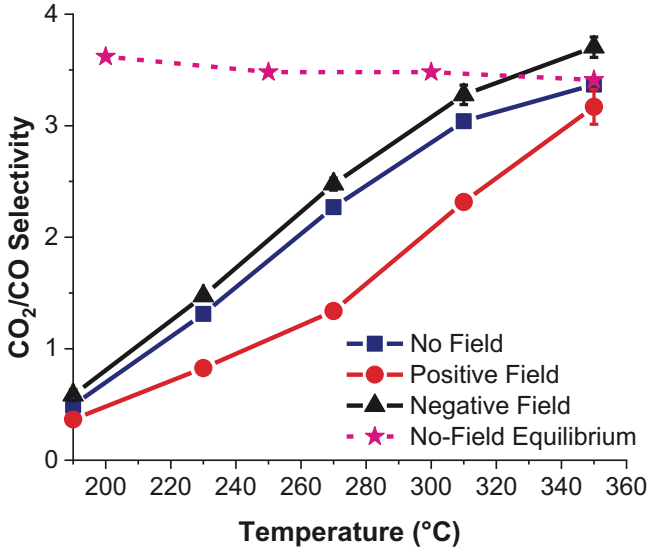

Fig. 5. Changes in CO_2/CO selectivity for FA decomposition over a single Ni foam disk (equilibrium data measured over excess catalyst) as functions of temperature and applied field.

operating parameters to test the field-amplified sample, it must be recognized that the single-disk design of the field-amplified catalytic reactor is still subject to a number of limitations which limit its usability as an ideal catalytic test setup (mass transfer limitations, for example). As the focus of this work is not on reactor design but rather a characterization of a previously existing reactor under the applied electric field, this no-field equilibrium line shown in Fig. 5 represents the closest to true equilibrium that can be achieved with the limitations set. According to Fig. 5, thermodynamic equilibrium across one catalyst disk is achieved at 350 °C. This is most likely due to the reaction being kinetically controlled at the lower temperatures. Temperatures above 350 °C were not tested to minimize interference from reactions with the reactor walls and gas-phase decomposition which start to become apparent between 350 and 400 °C according to reactor blank tests. Since our mathematical treatment (i.e., Eq. (9)) focuses only on the thermodynamic effects of an electric field, only the experimental data obtained at 350 °C were used for the analysis of Eq. (9) to back-calculate the average electric field strength over the catalyst surface. This was done simply by solving for F in Eq. (9) by rewriting as a quadratic expression and implementing the quadratic formula:

$$0 = (\Delta\Delta\alpha)F^2 + 2(\Delta\Delta\mu)F - 4k_B T \ln\left(\frac{S}{S_0}\right) \tag{10}$$

$$F = \frac{-(\Delta\Delta\mu) \pm \sqrt{(\Delta\Delta\mu)^2 + 4(\Delta\Delta\alpha)k_B T \ln(S/S_0)}}{(\Delta\Delta\alpha)} \tag{11}$$

where $\Delta\Delta\mu$ and $\Delta\Delta\alpha$ refer to the quantities $(\Delta\mu_1\text{-}\Delta\mu_2)$ and $(\Delta\alpha_1\text{-}\Delta\alpha_2)$ in Eq. (9), respectively.

As might be expected by comparing the selectivity data at 350 °C from Figs. 4 and 5, the small changes in selectivity when the field is applied corresponds to a low electric field—on the order of 0.2 V/nm. It should be noted that this field is not reflective of the entire surface, but only those sites that are the most reactive on the catalyst surface. It is therefore slightly inaccurate to think of this computed field value as an average over the entire surface and should be more accurately described as an average over the *catalytically active sites*. However, since the catalyst active sites are difficult to precisely pin down, we assume for subsequent analysis that these numbers represent an average over the entire surface with the explicit understanding that this is an inherently inaccurate model.

3.4. COMSOL modeling

To verify the estimates of the surface electric field strengths from our reactive formic acid probe measurements, we modeled the catalyst system in COMSOL as shown in Fig. 6. This model indicates that the role of added particles to the foam is twofold: first, adding particles helps to distribute the field more evenly across the catalyst surface and, second, that the particles increase the average field strength by 3–4 orders of magnitude. Fields on the surface of a metallic foam with no particles tend to be concentrated around the wire leading to the external circuit, diminishing rapidly toward the edge of the plate. Adding particles into the pores, however, changes the structure of the field such that it is more evenly distributed across the catalyst. Furthermore, the fields tend to be concentrated on the pore edges and particle surfaces, where catalyst active sites are most likely located.

Most importantly, the magnitude of the electric field produced is expected to increase by several orders of magnitude. Depending on the location within the foam catalyst, the field strength increases by 1 (on the top surface, excluding pores) to 3 orders of magnitude (inside the pore walls). The field is still higher on the surface of the particles, being at least 1 order of magnitude higher than even the pore wall field. Average electric field values on different portions of the model are shown in Table 2. These apparent surface electric field enhancements within the pore walls and over the surface of particles indicate that both surface curvature and particle confinement effects can enhance the magnitude of the surface electric field over the metal foam. Increasing the roughness of the surface by the addition of particles has an amplifying effect on the field as charges selectively move into sharp points and bumps on the surface to minimize crowding and charge-charge interactions [32,33]. More charges in these small areas lead to increased electric field strengths at these points. Hence, the areas of greatest field strength are expected to be bumps, defects, edges, and similar places. By applying these curvature and particle confinement effects into the reactor design, it is very possible to create the high surface electric field without applying the high external voltage.

While the COMSOL model provides interesting insight and added confidence in the overall field *structure*, it disagrees with the field

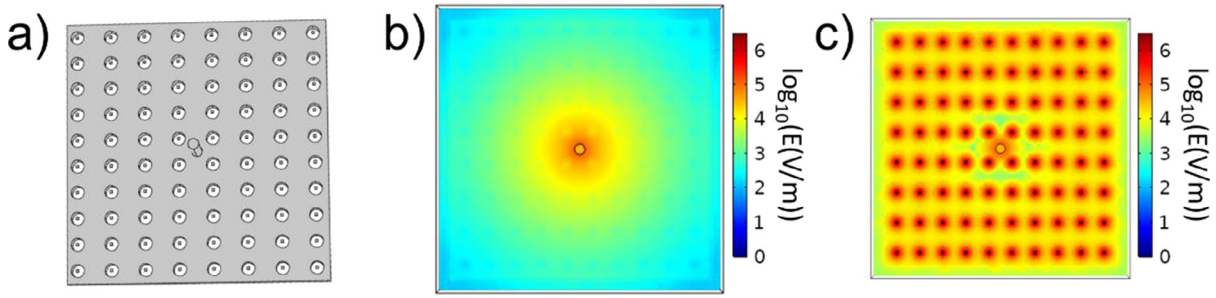

Fig. 6. COMSOL results of the surface electric field for a piece of metallic Ni foam connected to an electrical circuit with 200 V applied potential and 1 μA current. (a) The geometry used for this model, which was tested (b) without and (c) with the addition of microparticles in the foam pores.

Table 2
Surface electric fields taken at different locations in the COMSOL model of the foam catalysts.

Location of measurement	Surface field strength (V/m)	
	Foam only	Foam and particles
Top surface not including area inside pore	2245	20,377
Side walls of a random pore	72.906	28,830
On surface of a particle	–	816,600

magnitudes estimated by the FA decomposition tests (0.2 V/nm or 2.0×10^8 V/m). One reason for this is the simplified nature of the simulation. Although the enhanced field is strongly dependent on the presence of microparticles, the particle concentration is much lower in the model compared to the experimental catalyst. Additionally, the location of the particles further affects the enhanced field through pore wall-particle and particle–particle gap distances which are more complex in reality than in the model. Furthermore, the real system contains many physical defects (kinks, holes, protrusions, crystallite domain boundaries, lumps, and sharp points) that will greatly enhance the surface field and are not accounted for in this idealized model. Nevertheless, the COMSOL model clearly indicates the expected location and distribution of the strongest surface electric fields. For example, the surface electric field was the strongest on the surface of particles that are located within the micropores of the metal foam.

3.5. Field visualization by electron microscopy

Imaging the catalyst with and without the externally applied field in an electron microscope was used to verify if the field lines were concentrated at pore edges and particle defects as suspected. Correlating the average brightness of the surface measured by SEM with the average measured field strength from the formic acid decomposition reaction allows for an order-of-magnitude approximate visualization of the applied field during the reaction. One such visualization of a particle in a pore is provided in Fig. 7. Of particular interest are the edges of the pore and the surface of the particle. As expected from our COMSOL analysis, the pore edges and rough points of the particle exhibit the most substantial changes in brightness and, therefore, the highest local potential or surface field strength.

In principle several factors aside from the applied voltage itself could contribute to brightness changes during SEM imaging of an electrified sample. For example, field evaporation of the metal structure may occur over sharp points at high enough applied fields which can cause brightness changes due simply to a change in the structure itself. Alternatively, material changes due to contamination (e.g., coking) by the reactive materials presented in the atmosphere may cause subtle changes in the brightness. Furthermore, as high electric fields are applied to a sample (particularly one with a high degree of heterogeneity), it can be expected that the structure will experience some degree of restructuring including ion migration and segregation of metal atoms. This restructuring effect can influence the brightness of an SEM sample. However, these effects are assumed to be negligible in their contributions to the brightness changes observed in the present study due to the relatively large dimensions of the sample (compared to, for example, the nanodimensional materials used in field ion microscopy which experience severe field evaporation), the short times involved in the imaging tests (fields are only applied for as long as the image takes to collect), the high vacuum used for imaging (10–6 torr), and high purity sample (99.5% Ni) used for imaging. Future research with environmental SEM or nanodimensional materials should be aware of these effects.

Generating these “electric field maps” also allows for an estimation of the *maximum* electric field generated in our system, as opposed to the *average* electric field obtained from the formic acid reaction data. In the case of the maps given in Fig. 7, the maximum negative field is approximately −1.5 V/nm and the maximum positive field is +0.5 V/nm.

4. Conclusions

The straightforward chemistry of gas-phase formic acid decomposition over Ni foam and particle catalysts has been used to investigate the effects of an electric field on heterogeneous catalytic reactions. By using an integrated circuit reactor design consisting of a capacitor and a DC power source, unidirectional electric fields were generated on the surface of the catalyst without (*i*) generating plasma, (*ii*) promoting Faraday reactions, and (*iii*) causing Joule heating. Our thermodynamic calculations show that the magnitude of the selectivity for the formic acid decomposition reaction changes as a function of both the surface electric field strength and reaction temperature. This thermodynamic calculation indicates that positive fields should favor the production of CO/H_2O (via the dehydration pathway) while negative fields should

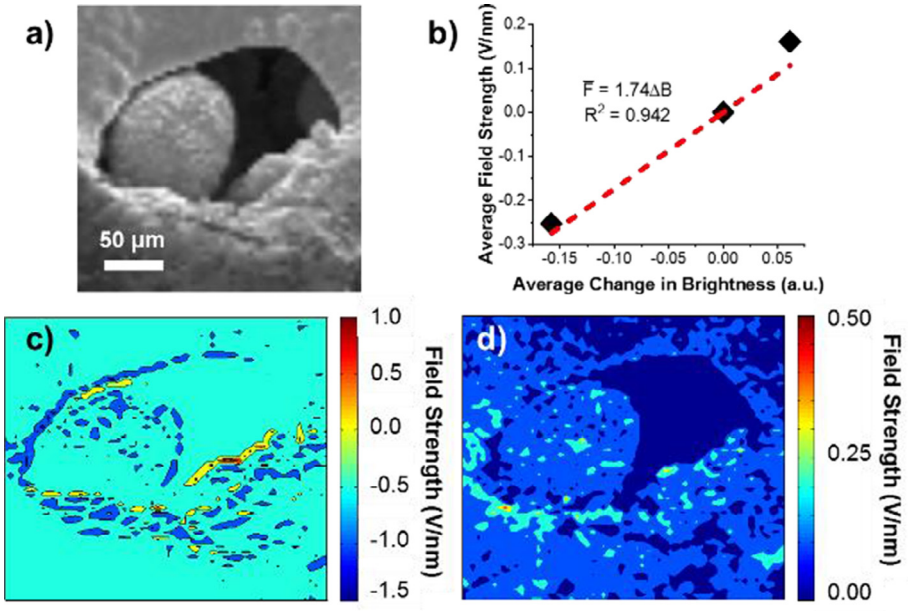

Fig. 7. SEM electric field mapping results for a Ni foam catalyst with microparticles. (a) An unaltered SEM image of a single particle in a pore, (b) the calibration curve generated by comparing average changes in brightness from SEM to the field strength estimated from HCOOH reaction. “Topographical maps” of the same particle in a pore with a (c) negative and (d) positive applied bias.

improve the production rates of CO_2/H_2 (via the decarboxylation pathway). The selectivity of the formic acid decomposition reaction was experimentally measured using our integrated circuit reactor, which confirms our thermodynamic calculation results that positive fields favor dehydration ($HCOOH \longrightarrow H_2O + CO$) while negative fields favor decarboxylation ($HCOOH \longrightarrow CO_2 + H_2$). Finally, a change in the average brightness of the Ni foam surface measured by SEM due to the applied electric bias was correlated to the average measured field strength from the formic acid decomposition reaction. Such correlation allows for an order-of-magnitude approximate visualization of the applied field over Ni foam catalyst during the reaction. Imaging the catalyst with and without the externally applied field in SEM was used to verify that the field lines were concentrated at pore edges and particle defects as predicted by our COMSOL model.

Declaration of Competing Interest

The authors declare the following financial interests/personal relationships which may be considered as potential competing interests: Dr. Yang from KIER is the co-author of this manuscript and KIER has funded a part of the researches presented in this manuscript.

Acknowledgements

This material is based upon work supported by the National Science Foundation Graduate Research Fellowship under Grant No. 1347973. Funding by the Research and Development Program of the Korea Institute of Energy Research (KIER) (No. C0-2420), Republic of Korea is also gratefully acknowledged. Special thanks to the Franceschi Microscopy and Imaging Center (FMIC) at WSU for the use of their electron microscope expertise and facilities. K.A. and J.H.C. acknowledge the Minnesota Supercomputing Institute (MSI) at the University of Minnesota for providing computational resources. This work was partially supported by the National Science Foundation through the University of Minnesota MRSEC under Award Number DMR-1420013.

Appendix A. Supplementary data

Supplementary data to this article can be found online at https://doi.org/10.1016/j.cej.2020.125640.

References

[1] K. Bergmann, M. Eigen, L. De Maeyer, Dielektrische absorption als folge chemischer relaxation, Berichte der Bunsengesellschaft Phys. Chem. 67 (8) (1963) 819–826.
[2] L.C.M. De Maeyer, [4] Electric field methods, Methods Enzymol. 16 (1969) 80–118.
[3] Abend, G., R.-G. Abitz, and J.H. Block, Influences of high electric fields on surface reactions of sulfur on metals. Investigated by field desorption, in Proceedings of the 31st International Meeting of the Societe de Chimie Physique. 1978. p. 261-263.
[4] H.J. Kreuzer, R.L.C. Wang, Physics and chemistry in high electric fields, Philos. Mag. Part B 69 (5) (1994) 945–955.
[5] Kreuzer, H.J., Chemical Reactions in High Electric Fields, in Surface Science of Catalysis. 1992, American Chemical Society. p. 268-286.
[6] J.H. Block, Chemical surface reactions in the presence of high electric fields, C R C Crit. Rev. Solid State Sci. 6 (2) (1976) 133–156.
[7] L. Hellemans, L.D. Maeyer, Absorption and dispersion of the field induced dielectric increment in caprolactam–cyclohexane solutions, J. Chem. Phys. 63 (8) (1975) 3490–3498.
[8] F. Che, et al., Catalytic water dehydrogenation and formation on nickel: Dual path mechanism in high electric fields, J. Catal. 332 (2015) 187–200.
[9] F. Che, et al., Improving Ni catalysts using electric fields: a DFT and experimental study of the methane steam reforming reaction, ACS Catal. 7 (1) (2017) 551–562.
[10] F. Che, et al., Reducing reaction temperature, steam requirements, and coke formation during methane steam reforming using electric fields: a microkinetic modeling and experimental study, ACS Catal. (2017).
[11] M.M. Aleksankin, V.V. Lobanov, Quantum chemical investigation of the behaviour of molecules and their ions in an electric field: I Propanal, Int. J. Mass Spectrom. Ion Phys. 15 (1) (1974) 1–8.
[12] V.V. Lobanov, M.M. Aleksankin, Y.A. Kruglyak, Quantum chemical investigation of molecule and ion behaviour in an electric field. II. Ethanal, Int. J. Mass Spectrom. Ion Phys. 18 (4) (1975) 275–288.
[13] Chuah, G.-K., et al., ELECTROSTATIC FIELD EFFECTS ON INTERMEDIATES OF CATALYTIC SURFACE REACTIONS. J. Phys. Colloques, 1987. 48(C6): p. C6-493-C6-498.
[14] N. Kruse, et al., Decomposition of methanol over Rh and Ru, Surf. Sci. 189–190 (1987) 832–841.
[15] D.L. Cocke, et al., Copper oxidation and surface copper oxide stability investigated by pulsed field desorption mass spectrometry, Appl. Surf. Sci. 84 (2) (1995) 153–161.
[16] J.S. McEwen, et al., Field-assisted oxidation of rhodium, Chem. Phys. Lett. 452 (1–3) (2008) 133–138.
[17] B.N.J. Persson, P. Avouris, The effects of the electric field in the STM on excitation localization. Implications for local bond breaking, Chem. Phys. Lett. 242 (4) (1995) 483–489.
[18] M. Alemani, et al., Electric field-induced isomerization of azobenzene by STM, J. Am. Chem. Soc. 128 (45) (2006) 14446–14447.
[19] A.C. Aragonès, et al., Electrostatic catalysis of a Diels-Alder reaction, Nature 531 (7592) (2016) 88–91.
[20] S. Shaik, D. Mandal, R. Ramanan, Oriented electric fields as future smart reagents in chemistry, Nat. Chem. 8 (2016) 1091.
[21] F. Che, et al., Elucidating the roles of electric fields in catalysis: a perspective, ACS Catal. 8 (6) (2018) 5153–5174.
[22] M. Stoukides, C.G. Vayenas, The effect of electrochemical oxygen pumping on the rate and selectivity of ethylene oxidation on polycrystalline silver, J. Catal. 70 (1981) 137–146.
[23] N.A. Anastasijevic, NEMCA—From discovery to technology, Catal. Today 146 (3) (2009) 308–311.
[24] M.Y.A. Mollah, et al., Plasma chemistry as a tool for green chemistry, environmental analysis and waste management, J. Hazard. Mater. 79 (3) (2000) 301–320.
[25] Parvulescu, V.I., M. Magureanu, and P. Lukes, Plasma Chemistry and Catalysis in Gases and Liquids. 2013: Wiley.
[26] A.K.T. Assis, W.A. Rodrigues, A.J. Mania, The electric field outside a stationary resistive wire carrying a constant current, Found. Phys. 29 (5) (1999) 729–753.
[27] M.A. Heald, Electric fields and charges in elementary circuits, Am. J. Phys. 52 (6) (1984) 522–526.
[28] N.W. Preyer, Surface charges and fields of simple circuits, Am. J. Phys. 68 (11) (2000) 1002–1006.
[29] O. Jefimenko, Demonstration of the electric fields of current-carrying conductors, Am. J. Phys. 30 (1) (1962) 19–21.
[30] Jacobs, R., A.d. Salazar, and A. Nassar, New experimental method of visualizing the electric field due to surface charges on circuit elements. American Journal of Physics, 2010. 78(12): p. 1432-1433.
[31] J.T. Gray, et al., Field-assisted suppression of coke in the methane steam reforming reaction, Appl. Catal. B 260 (2020) 118132.
[32] Ruppin, R., Electric field enhancement near a surface bump, 1981, 39, 8, 903-906.
[33] Brailsford, D.F. and Robertson, A.J.B., Calculation of electric field strengths at a sharp edge, 1968. 1, 1, 75-85.